Dynamics and mechanism of a deswelling transition of the sponge phase in a bilayer membrane system

Rei Kurita,* Takumi Kanazawa, Yukihiro Terada, and Marie Tani
Department of Physics, Tokyo Metropolitan University, 1-1 Minamioosawa, Hachiouji-shi, Tokyo 192-0397, Japan

(Received 21 February 2022; accepted 13 June 2022; published 29 June 2022)

In surfactant solutions, membranes are self-organized and divide water into two domains, an "inside" and an "outside." When the membrane phase transforms into a dilute sponge (L_1) phase, the L_1 phase is also partitioned into inside and outside domains. Such systems are critical not only for material exchange mechanisms in biology but also for the formation of boundaries between topologically distinct regions. Nevertheless, the mechanism and associated behavior of the system at the transition remain unclear. Here, we use both experimental observations and numerical simulations to investigate the phase transition dynamics. It is found that domains of inside and outside are formed which appear connected to each other and that they nucleate as droplets despite the L_1 phase being the majority phase. Although such behavior is significantly different from what is seen in ordinary phase separation, we successfully reproduced all typical behavior seen in the experiments with numerical simulations. For the formation of the connected domains, it is found that the correlation length associated with the concentration needs to be larger than that of the inside/outside patterns. This offers a means to control pattern formation in systems with a parity mechanism, such as chirality.

DOI: 10.1103/PhysRevResearch.4.023254

I. INTRODUCTION

Membranes play an important role in the function of biological organisms. For example, lateral diffusion in membranes is crucial for the transport of materials such as polymers, colloids, and proteins [1–3]. Meanwhile, material transport *through* membranes also occurs, controlled by the assembly of pores [4,5]. To understand the physics of membrane transport, model systems of surfactant solutions have been widely studied [6–14]. In aqueous surfactant solutions, stable bilayer membranes are formed by amphiphilic molecules under certain conditions. Membranes may also form higher-order structures such as vesicles, lamellae, and sponges [7,11]. Such structures are formed by long-range interactions known as Helfrich interactions, a result of electrostatic and steric repulsion [6].

Studies of surfactant solutions have revealed many unique features and phases of membranes. A sponge phase in aqueous solution, for example, features an infinite bilayer membrane of complex topology. The membrane divides space into two distinguishable regions [8,9], arbitrarily classified as "inside" and "outside." Using a field representation, we may denote the inside and outside domains as having parameter values of $\eta = 1$ and -1, respectively. Note that η resembles parity since it seems that both domains are energetically equivalent. When the total volume of space where $\eta = 1$ is equal to where $\eta = -1$, the system is in a symmetric (S) sponge phase; when they are different, the system is in an asymmetric (A) sponge phase [8,9]. It was reported that the results of certain scattering experiments suggest the existence of an S-A transition, where the symmetry between the parities is broken [8]. Such a transition would suggest there is an exchange of water though the membranes. Despite crucial implications for both physics and biology, however, it still remains unclear which systems might exhibit such a transition.

Regions where $\eta = \pm 1$ can be directly visible under optical microscopy when the deswelling transition from an isotropic sponge phase into a coexistence phase of a hyperswollen sponge phase (L_1 phase) and a dense sponge phase (L_3 phase) occurs. The status $\eta = \pm 1$ is transferred to the L_1 phase; thus, the L_1 phase is also divided into two phases. In a $C_{10}E_3$ solution with dispersed colloidal particles [10], it was reported that the colloidal particles are exclusively localized in $\eta = 1$ (or $\eta = -1$) domains. Such results indicate a clear distinction between $\eta = \pm 1$ domains, and they suggest the existence of an S-A transition. Yet whether this residence is induced by the S-A transition or by a particle effect is important. It was also reported that the S-A transition in the sponge phase could not be observed by light scattering when the solution does not contain colloidal particles [10]. These results suggest that the S-A transition in the $C_{10}E_3$ solution should be induced by mixing the colloidal particles. As a first step, the existence of an S-A transition in the $C_{10}E_3$ solutions without colloidal particles needs to be examined in more detail.

One key aspect of such a study would be the dynamics of the transition such as pattern formation, which is sensitive to initial conditions. For example, in ordinary phase separation, a droplet pattern is formed if the initial concentration is asymmetric, but a bicontinuous pattern is formed if it is symmetric [15]. According to previous research using $C_{10}E_3$ solutions [10], the emergence of connected

*Author to whom correspondence should be addressed: kurita@tmu.ac.jp

droplets of $\eta = \pm 1$ domains was observed. It is expected that the typical dynamics of the pattern evolution may reflect whether the sponge phase is symmetric or asymmetric. Furthermore, this dynamics might be connected to other systems with parity such as cholesteric liquid crystals [16] and crystals with chirality [17]. Since boundaries between the different parity domains have unique physical properties such as topological insulation [18], understanding the mechanism behind the formation of such connected domains may also lead to the development of new applications. Thus, it is crucial to phenomenologically clarify the dynamics and mechanism behind the transition from the sponge phase to the coexistence phase not only to verify the existence of an *S-A* transition in surfactant systems but also to understand the formation of topological boundaries in systems with parity.

Here, we investigate the dynamics of the transition, i.e., the pattern formation and coarsening process in a $C_{10}E_3$ solution. In addition, we perform numerical simulations based on a phenomenological equation, finding that the experimental observations are reproduced numerically. Comparing the experimental results with the simulation, it was found that the sponge phase remains symmetric in the $C_{10}E_3$ solution and that the ratio between different correlation lengths associated with the concentration and the inside/outside patterns is critical for the formation of connected droplets of different parity domains.

II. EXPERIMENTS

A. Materials and methods

The surfactant we used was the nonionic surfactant $C_{10}E_3$ (triethylene glycol mono-*n*-decyl ether, Nikko Chemicals Inc., BD-3SY). A 3.0 wt% concentration solution was prepared using pure water as a solvent. When the surfactant molecules are dissolved into water, they spontaneously form bilayer membranes at room temperature. The bilayer membranes go on to form higher-order structures, making them a popular lyotropic liquid crystal (LC) system. A phase diagram for $C_{10}E_3$ is shown in Fig. 1. Here, we briefly review the phase diagram at 3.0 wt %. At 20.0 °C, membranes form a lamellar phase (L_α, smectic LC) with a one-dimensional periodic order of surfactant bilayers. When $T > 32.0$ °C, they form a sponge phase (L_3, isotropic fluid), a random bicontinuous structure of membranes and water [4]. At a transition temperature $T_c = 32.9$ °C, the sponge phase transforms into a coexistence phase consisting of an L_1 phase and a dense L_3 phase. We note that the concentration of the L_1 phase is quite low (<0.1%) [11]. In the coexistence region, the volume fractions are determined from the phase diagram, following the lever rule. The dashed line shown in Fig. 1 corresponds to a symmetrical line where the volume fractions of L_1 and L_3 are the same. L_3 is a majority phase when T_a is below the symmetrical line, while L_1 is the majority phase if T_a is above the symmetrical line.

For most cases, we confined a sample between two parallel cover glasses spaced about 5 μm apart. To prevent evaporation, the sample was sealed with an ultraviolet light-curable adhesive (NOA68, THORLABS). Next, the sample was annealed at $T = 32.5$ °C for 30 min to prepare a homogeneous sponge phase (shown by the filled circle). Finally, the sample

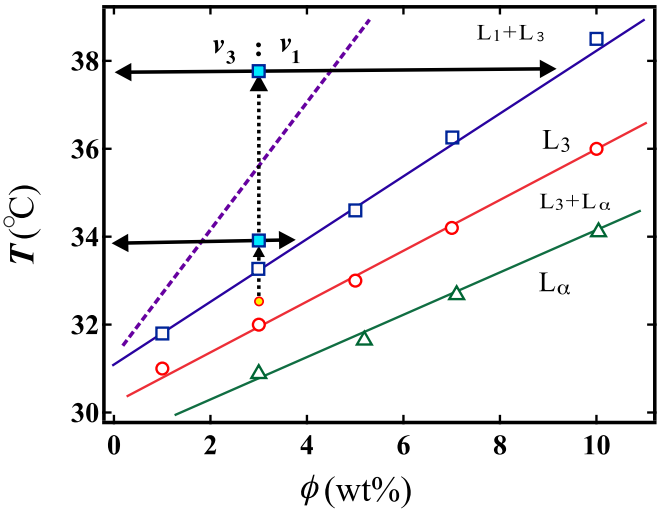

FIG. 1. Phase diagram of $C_{10}E_3$ solutions. Symbols are measurement points, and solid lines are linear fittings. The triangles and green line correspond to the transition temperature from the lamella phase (L_α) to the coexistence phase of L_α and the sponge phase (L_3). The open circles and red line correspond to the transition temperature from the $L_\alpha + L_3$ phase to the L_3 phase. The open squares and blue line correspond to the transition temperature from the L_3 phase to the coexistence phase of L_3 and the L_1 phase. In the coexistence region, the volume fractions (v_1 for L_1 and v_3 for L_3) are determined from the phase diagram, following the lever rule. The purple dashed line corresponds to a symmetrical line where the volume fractions of L_1 and L_3 are the same. Thus, L_3 is a majority phase when T_a is below the symmetrical line; on the other hand, L_1 is the majority phase if T_a is above the symmetrical line. We annealed samples at $T = 32.5$ °C, shown by the filled circle in the L_3 phase, to prepare a homogeneous sponge phase. Then the sample was heated rapidly to a target annealing temperature T_a, shown by the filled squares.

was heated rapidly to a target annealing temperature T_a at a speed of 12.0 °C/min, taking the system into the L_1/L_3 coexistence region. We controlled the temperature using a hot stage (10021, Linkam). The hot stage is enclosed by an acrylic box; thus, a temperature gradient can be neglected. Overshooting of the temperature during the heating process is less than 0.1 °C, and the temperature relaxes to T_a within 0.3 s. We set $t = 0$ at the time when the temperature relaxes to T_a. An equilibrium time of the sample temperature is estimated to be less than 0.1 s using the thermal diffusion equation. To obtain this, we used the fact that the thicknesses of the cover glass and water were 140 and 5 μm, respectively. We also used thermal diffusion constants of the glass and water of 4.3×10^{-7} and 1.4×10^{-7} m^2/s, respectively. To make sure the estimation of the equilibrium time, we performed a numerical calculation of the thermal diffusion equation, and we ensured that the equilibrium time was less than 0.1 s. Then we observed the transition dynamics using phase contrast microscopy (ECLIPSE TS100-F, Nikon). We took images with a CCD camera attached to the microscope at a rate of 1 frame/s for the early stage of the transition and 1 frame/5 min for the later stage.

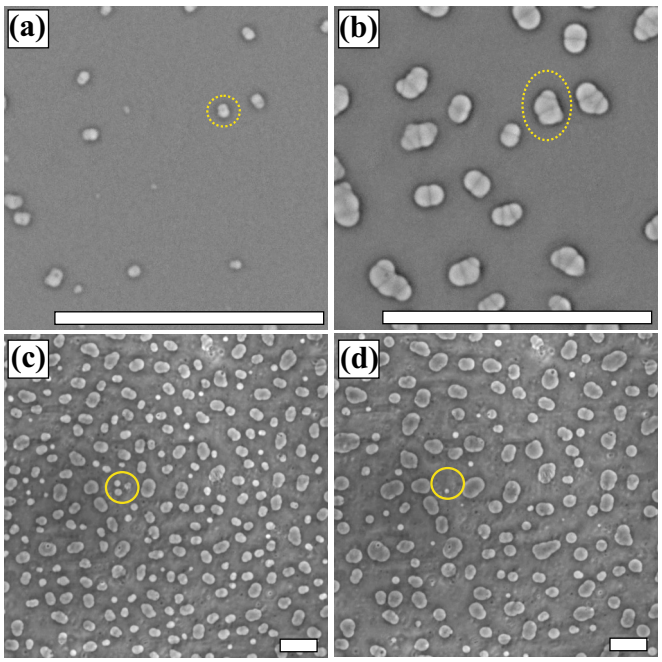

FIG. 2. The transition behavior at $\Delta T = 1$ °C at (a) $t = 40$ s, (b) 155 s, (c) 2555 s, and (d) 7655 s. Nuclei of the L_1 phase appear as two-domain droplets. In the dotted circles in (a) and (b), another L_1 droplet is nucleated onto the side of an existing two-domain droplet. Later, during the coarsening process, we observed a small, two-domain droplet first become a small, single droplet before it disappeared, as shown by the solid circles in (c) and (d). The white bar corresponds to 100 μm.

B. Transition behavior near the binodal line

First, we use phase contrast microscopy to observe the transition from the sponge phase to the L_1/L_3 coexistence phase near the binodal line. Figure 2 shows the time evolution of the system at $\Delta T = T_a - T_c = 1$ °C, where T_a and T_c are the annealing temperature and the transition temperature, respectively (see Movie S1 in the Supplemental Material [19]). In the early stages of the transition, most nuclei of the L_1 phase (>90%) appear to consist of two connected droplets [Fig. 2(a)]. These domains seem to consist of both inside ($\eta = 1$) and outside ($\eta = -1$) L_1 phases. As time elapses, these two-domain droplets become n-domain droplets, where n is an integer greater than 2. This occurs via two pathways: another L_1 droplet may be nucleated onto the side of a two-domain droplet [Fig. 2(b)], or a two-domain droplet collides with another two-domain droplet. In the latter case, the domains are fused if the parities of the L_1 domains that collide are the same; on the other hand, the domains are still separated if the parities are different. At a later stage, when we see coarsening, small droplets tend to disappear, while large ones become even larger [e.g., the droplets in the solid circles in Figs. 2(c) and 2(d)]. This coarsening process seems to be a Landau-Lifshitz growth process [15,20].

Next, we analyzed the time evolution as the pattern coarsens. Figure 3 shows the mean size of the droplets as a function of time at $\Delta T = 1$ °C. Circles correspond to the mean size of n-domain droplets without distinguishing separated domains, while triangles correspond to the mean size of each separated domain. It is found that both droplet sizes scale as $t^{1/3}$ (solid lines in Fig. 3). This exponent is the same as that expected for coarsening in phase separation with a conserved order parameter [15,20]. In this surfactant system, it is known that the characteristic time for the exchange of water from inside to outside (or from outside to inside) domains is quite long [10]. Thus, the parity parameter η can be treated as the conserved parameter, consistent with a $t^{1/3}$ growth process.

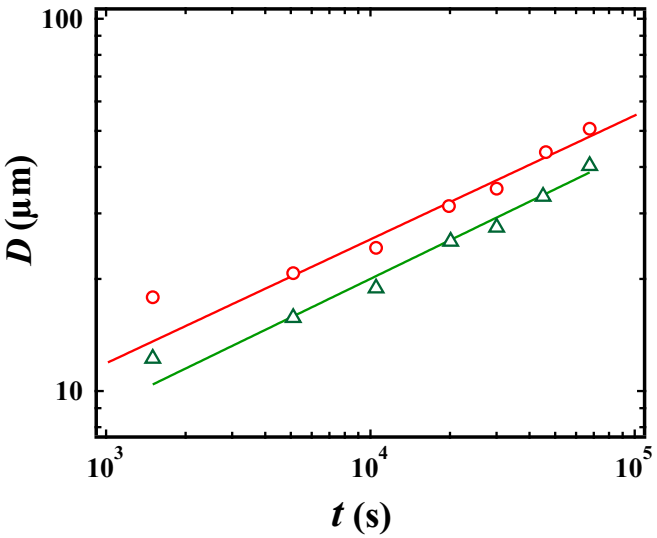

FIG. 3. Mean size of the droplets as a function of time at $\Delta T = 1$ °C. Circles show the mean size of the droplets without distinguishing separated domains, while triangles correspond to the mean size of each separated domain. Solid lines correspond to $t^{1/3}$.

C. Transition behavior far from the binodal line

Next, we observe the transition dynamics far from the binodal line. In this case, the L_1 phase is the majority phase; that is, the area of the L_1 phase is larger than that of the L_3 phase (see Fig. 1). Figure 4 shows the time evolution of the transition at $\Delta T = 5$ °C. In the very early stage, it is observed that fluctuations in intensity increase over time (see Movie S2 in the Supplemental Material [19]). This is similar to the typical spinodal decomposition seen during phase separation. However, it is observed that a nucleus of the L_1 phase suddenly appears [dotted line in Fig. 4(a)]. We note that a domain with a low refractive index has brighter intensity in our phase contrast microscopy images. It is thus clear that the nucleus consists of the L_1 phase; the L_1 phase has a lower refractive index than the L_3 phase (see Fig. 2). This is unexpected for two reasons. First, nucleation is never observed during ordinary spinodal phase separation; second, the "majority" phase does not nucleate in the minority phase during normal phase separation. We note that it takes approximately 25 s to reach ΔT of 5 °C, which is comparable to the dynamics of the transition. Here, the L_1 nucleus cannot be observed at $t = 0$ when the temperature reaches T_a. Once the L_1 phase emerges, the L_1 phase quickly grows with time (see Movie S2 in the Supplemental Material [19]). Thus, the possibility

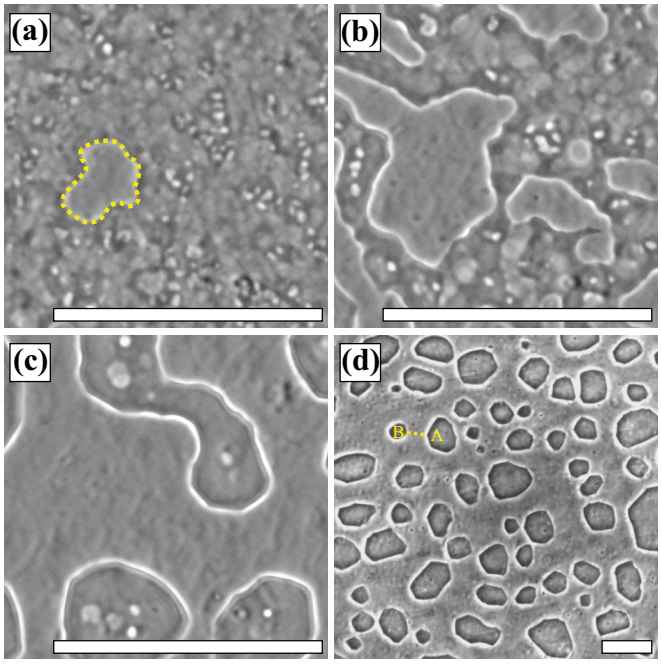

FIG. 4. The transition behavior at $\Delta T = 5$ °C at (a) $t = 9.5$ s, (b) 12.5 s, (c) 48.5 s, and (d) 13 600 s. The region surrounded by the dotted line in (a) shows a nucleus of the L_1 phase. (b) The region grows over time, before (c) the L_1 phase percolates. Even though it is the majority phase, the L_1 phase nucleates in the minority phase, which is distinct from ordinary phase separation. At 13 600 s, the droplets of the L_3 phase are polygonal rather than spherical. In this dynamics, self-similarity is breaking. The points indicated as A and B are connected by a domain-separating membrane (dotted line) under tension in the L_1 phase. The white bar corresponds to 100 μm.

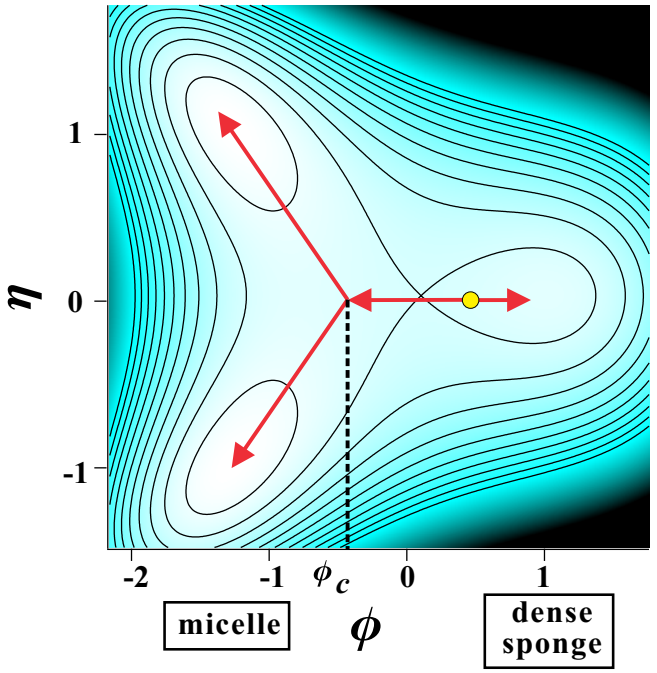

FIG. 5. Contour plot of $F(r)$ when $\alpha = 1$. Brighter color corresponds to lower free energy. The circle denotes the initial condition. The arrows correspond to the dynamical paths of the transition. The paths bifurcate at $\phi < \phi_c$, and η splits into ± 1.

that the minute L_1 nucleus is formed during the heating can be ruled out. Meanwhile, the spinodal decomposition may proceed during the heating. The L_1 domain grows over time [Fig. 4(b)] before it finally percolates [Fig. 4(c)], confirming that it is, indeed, the majority phase. It is also found that self-similarity of the pattern is broken during the transition. We also observe the pattern at 13 600 s, when the system is nearly in a steady state [Fig. 4(d)]. It is interesting that the droplets of the L_3 phase are polygonal, not spherical. Here, we note that points on the edge of the L_3 phase [like those indicated in Fig. 4(d)] may be connected via a membrane separating the inside and outside domains in the L_1 phase. This membrane is under tension, pulling at the boundary of L_3 droplets and creating an attractive interaction. This is balanced by interfacial tension in the L_1/L_3 boundary, forming droplet boundaries with well-defined edges.

III. SIMULATIONS

Next, we proceeded to carry out numerical simulations to further our understanding of the dynamics of the transition going from the sponge phase to an L_1/L_3 coexistence phase.

A. Simulation methods

We use the time-dependent Landau-Ginzburg approach to compute the transition dynamics from the sponge phase to the coexistence phase. There are two order parameters: one (ϕ) corresponds to the difference of the surfactant concentration from the mean concentration, and the other (η) corresponds to the difference in the volume fraction between the inside and outside. $\bar{\eta}$ should be zero for the S sponge phase, while $\bar{\eta} \neq 0$ for the A phase. Following previous work [8,9,21], the free energy $F(r)$ is described as

$$F(r) = f(r) + g(r) + C\phi\eta^2, \tag{1}$$

$$f(r) = -\tfrac{1}{2}a\phi^2 + \tfrac{1}{4}b\phi^4 + \tfrac{1}{2}\gamma_\phi(\nabla\phi)^2, \tag{2}$$

$$g(r) = \tfrac{1}{2}A\eta^2 + \tfrac{1}{4}B\eta^4 + \tfrac{1}{2}\gamma_\eta(\nabla\eta)^2, \tag{3}$$

where $f(r)$ and $g(r)$ correspond to the free energy due to ϕ and η, respectively. For the L_1/L_3 transition, the constant a should be positive. The last term in the expansion of $F(r)$ shows coupling between ϕ and η to lowest order; η is squared since the inside and outside, i.e., $\eta = \pm 1$, domains should have the same free energy. Figure 5 shows the free energy described in Eq. (1) when C is positive. When C is positive, there are three minima: $(\phi, \eta) = (0.9, 0)$, $(-1.2, 1)$, and $(-1.2, -1)$. The minimum at $(\phi, \eta) = (0.9, 0)$ corresponds to the L_3 phase, while the minima at $(\phi, \eta) = (-1.2, 1)$ and $(-1.2, -1)$ correspond to the inside and outside domains of the L_1 phase, respectively.

Here, we assume that η is conserved since the timescale of the exchange of water between the inside and outside domains is much slower than the dynamics of the transition [10,14]. We then obtain the following kinetic equations for ϕ

and η:

$$\frac{\partial \phi}{\partial t} = L_\phi \nabla^2[-a\phi + b\phi^3 - \gamma_\phi \nabla^2 \phi + C\eta^2], \tag{4}$$

$$\frac{\partial \eta}{\partial t} = L_\eta \nabla^2[A\eta + B\eta^3 - \gamma_\eta \nabla^2 \eta + 2C\phi\eta], \tag{5}$$

where L_ϕ and L_η are transport coefficients. We can then define correlation lengths for ϕ and η as $\xi_\phi = \sqrt{\gamma_\phi/a}$ and $\xi_\eta = \sqrt{\gamma_\eta/A}$. We may also define a timescale for the transition as $\tau = \xi_\phi^2/L_\phi a$. We normalize lengths, times, ϕ, and η using ξ_ϕ, τ, $\phi_e = \sqrt{a/b}$, and $\eta_e = \sqrt{A/B}$, respectively. We then obtain the normalized kinetic equations below:

$$\frac{\partial \phi}{\partial t} = \nabla^2[-\phi + \phi^3 - \nabla^2 \phi + \alpha\eta^2], \tag{6}$$

$$\frac{\partial \eta}{\partial t} = \frac{L_\eta A}{L_\phi a}\nabla^2\left[\left(1 - \frac{\phi}{\phi_c}\right)\eta + \eta^3 - \frac{\xi_\eta^2}{\xi_\phi^2}\nabla^2\eta\right], \tag{7}$$

where $\alpha = C\eta_e^2/a\phi_e$ and $\phi_c = -A/2C\phi_e$. We set $\alpha = 1$, $\phi_c = -0.4$, and $L_\eta A/L_\phi a = 1$. Meanwhile, the mean of ϕ, $\bar{\phi}$; the mean of η, $\bar{\eta}$; and the ratio between the correlation lengths $\beta \equiv \xi_\phi/\xi_\eta$ are variable parameters. $\bar{\phi}$ corresponds to ΔT in our experiment since both parameters determine the area fractions of the L_1 phase and the L_3 phase. From a linear stability analysis, fluctuations in η become unstable when $\phi < \phi_c$ (see Fig. 5).

We performed the grain-coarsening simulation with a 512 $\times$ 512 simulation box. An initial condition for each simulation trial is prepared by using a random noise, and the time step for the simulation is set to 0.01.

B. Transition behavior when the L_3 phase is the majority phase

Here, we investigate the dynamics of the transition when the L_3 phase is the majority phase. Figures 6(a1)–6(a3) show the time evolution of $\eta(r)$ during the transition when $\bar{\phi} = 0.3$ and $\beta = 1$. First, we assume that the initial sponge phase is symmetric and set $\bar{\eta} = 0$. Isolated droplets appear at the early stage [Fig. 6(a1)]; this pattern is broadly preserved to later times [Figs. 6(a2) and 6(a3)]. The ratio of two-domain droplets is less than 20%, much lower than what was seen in experiments (see Fig. 2). Meanwhile, Figs. 6(b1)–6(b3) show the time evolution of $\eta(r)$ during the transition when $\bar{\phi} = 0.3$, $\bar{\eta} = 0.0$, and $\beta = 5$. Two-domain droplets appear at a very early stage [Fig. 6(b1)], and additional domains nucleate onto these droplets [Fig. 6(b2)]. We also observed two-domain droplets colliding with another droplet and fusing if η is the same at the collision point. This is the same as what was observed in experiment [see Fig. 2(b)]; that is, the simulation results when $\beta = 5$ and $\bar{\eta} = 0.0$ are consistent with experimental observations.

Furthermore, we computed the structure factor of η and located the peak at wave number q_m. Figure 7 shows the time evolution of q_m. The coarsening process starts after $t = 6000$, when q_m is seen to decrease over time with a fixed scaling. We see that $q_m \propto t^{-1/3}$. This is also consistent with the experimental results (see Fig. 3).

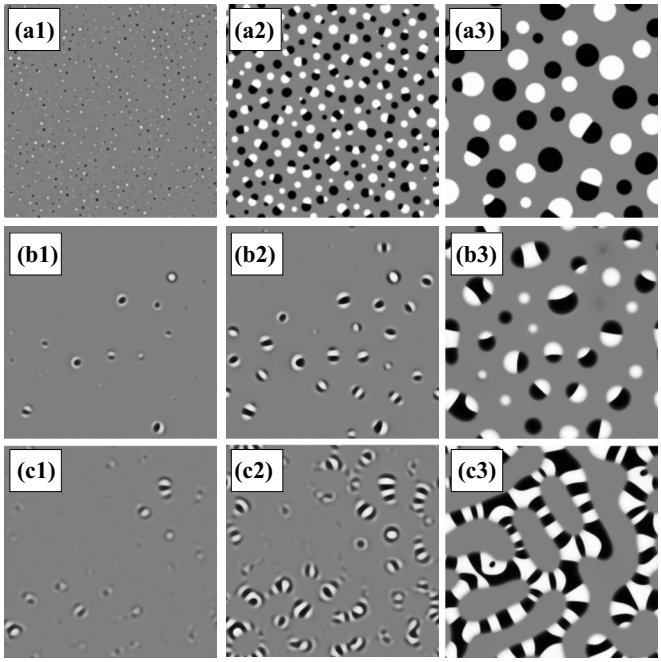

FIG. 6. (a) Pattern evolution when $\bar{\phi} = 0.3$, $\bar{\eta} = 0.0$, and $\beta = 1$ at (a1) $t = 130$, (a2) 2100, and (a3) 39 130. (b) Pattern evolution when $\bar{\phi} = 0.3$, $\bar{\eta} = 0.0$, and $\beta = 5$ at (b1) $t = 9000$, (b2) 10 180, and (b3) 38 620. (c) Pattern evolution when $\bar{\phi} = -0.3$, $\bar{\eta} = 0.0$, and $\beta = 5$ at (c1) $t = 8110$, (c2) 8480, and (c3) 38 660. White and black correspond to $\eta = 1$ and $\eta = -1$, respectively. The connected droplet pattern can be observed when β is large. It is also found that L_1 droplets appear even when the L_1 phase is the majority phase.

C. Transition behavior when the L_1 phase is the majority phase

Next, we show the time evolution when $\bar{\phi} = -0.3$, i.e., when the L_1 phase is the majority phase, $\bar{\eta} = 0.0$, and $\beta = 5$. This is given in Figs. 6(c1)–6(c3). This condition corresponds to $\Delta T = 5\,^\circ$C in our experiment (see Fig. 1). It is observed that nuclei of the L_1 phase appear at the early stages of the transition [Fig. 6(c1)], similar to what we see in our experiments

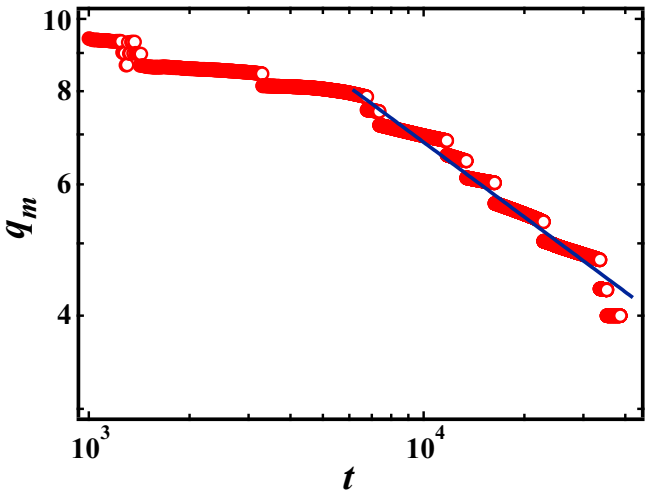

FIG. 7. Time evolution of q_m when $\bar{\phi} = 0.3$, $\bar{\eta} = 0.0$, and $\beta = 5$. The solid line corresponds to $t^{-1/3}$.

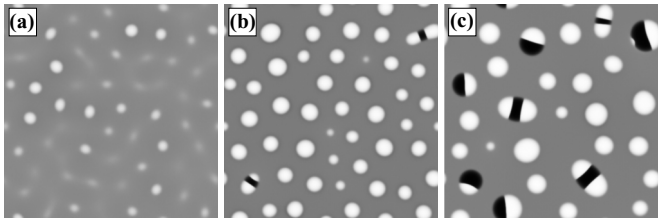

FIG. 8. Time evolution of η starting from an asymmetric sponge phase. We set $\bar{\phi} = 0.3$, $\bar{\eta} = 0.2$, and $\beta = 5$. (a) $t = 7310$, (b) 13 730, and (c) 38 560. At the early stage, only $\eta = 1$ droplets (white) are nucleated, with few partitioned droplets. $\eta = -1$ domains appear between the existing $\eta = 1$ droplets.

[Fig. 4(a1)]. New nuclei proceed to emerge on these droplets before they form n-domain droplets [Fig. 6(c2)]. Finally, the L_1 phase percolates the system, as shown in Fig. 6(c3). Such behavior closely aligns with our experimental results (see Fig. 4). It also indicates that the experimental results at $\Delta T = 5\ ^\circ$C are proper, rather than an experimental artifact.

From our simulation results, it can be concluded that the dynamical equation describes the transition dynamics when the ratio between the correlation lengths is large. We note here that the assumption $\xi_\phi \gg \xi_\eta$ is natural in a membrane system [9].

D. Transition behavior in the asymmetric sponge phase

Finally, we investigate the transition dynamics when the initial sponge phase is asymmetric, that is, $\bar{\eta} \neq 0$. Figure 8 shows the time evolution of η when $\bar{\phi} = 0.3$, $\bar{\eta} = 0.2$, and $\beta = 5$. At an early stage, only droplets with $\eta = 1$ are nucleated, and few partitioned droplets can be seen, as shown in Fig. 8(a). They grow over time, with domains of $\eta = -1$ appearing between the droplets where $\eta = 1$. This is not consistent with our experimental observations. Thus, this result suggests that the sponge phase is symmetric.

Here, it is worth noting that the symmetry of the sponge phase may easily be judged by observation of the transition from the sponge phase to the coexistence phase. The *S-A* transition was previously observed in a sodium dodecyl sulfate (SDS) + pentanol + water (salt) system [22]. The *S-A* transition occurs when the pentanol is mixed, but it does not occur by changing the temperature. Unfortunately, it is difficult to observe the dynamics in the SDS+pentanol+water (salt) system and to compare them with our simulation results. We think that in the future it will be important for this transition dynamics to be certified by finding a thermoinduced *S-A* transition.

IV. DISCUSSION

First, we discuss why a connected pattern is formed when the ratio between the correlation lengths is large. When a droplet of the L_1 phase nucleates, the interface length is proportional to the correlation length. Figures 9(a) and 9(b) show ϕ (red solid line) and η (blue dotted line) at the interface of a droplet with $\eta = 1$ when $\beta = 1$ and $\beta = 5$, respectively. Given an $\eta = 1$ droplet, two things are required for a two-domain droplet to form. First, fluctuations in η need to become unstable, making it more likely for a new droplet to nucleate. This is the case where $\phi < \phi_c$ (yellow shading). This region is particularly broad in the system with $\beta = 5$. Second, the newly nucleated droplet needs to be $\eta = -1$. This is more likely when $\eta < 0$ (blue shading). This region appears close to the interface since ξ_η is small. We note that there is an overlap region where $\phi < \phi_c$ and $\eta < 0$; this is a region where $\eta = -1$ droplets are particularly likely to nucleate. Note that the overlap region is quite narrow when $\beta = 1$, whereas it is much broader when $\beta = 5$. In addition, it is known that the energy barrier to nucleation drastically decreases with increasing correlation length [23–25]. Thus, when $\beta = 5$, a droplet with $\eta = -1$ nucleates close to the droplet with $\eta = 1$, leading to the emergence of two-domain droplets.

Next, we also discuss why droplets of the L_1 phase initially emerge in the L_3 phase when the L_1 phase is the majority phase. A spinodal decomposition of ϕ occurs prior to separation of η (see Fig. 5). ϕ becomes inhomogeneous, and regions where $\phi < \phi_c$ locally appear at some time, which is the same as ordinary spinodal decomposition. The separation

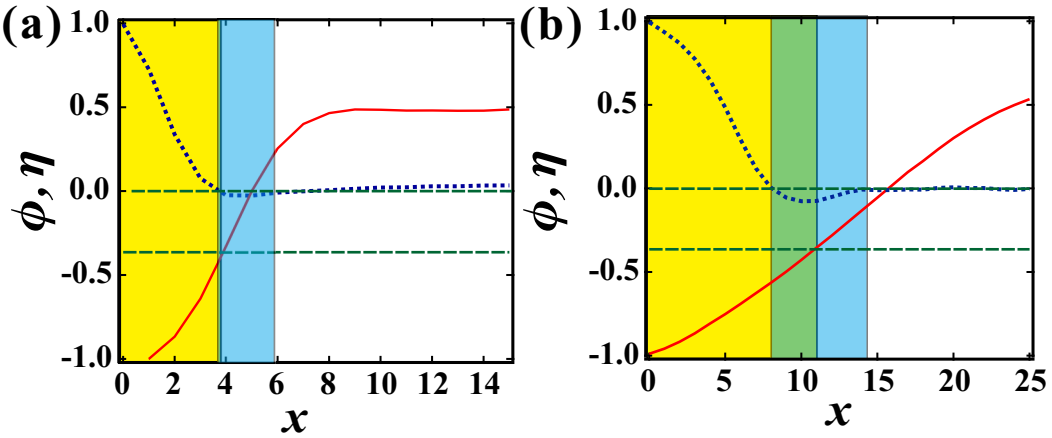

FIG. 9. ϕ (red solid line) and η (blue dotted line) at the interface of a droplet when (a) $\beta = 1$ and (b) $\beta = 5$. The dashed lines show $\phi = \phi_c$ and $\eta = 0$. A new micelle phase droplet is likely to be nucleated where $\phi < \phi_c$ (yellow). Meanwhile, when $\eta < 0$ (blue), the droplet is more likely to be $\eta = -1$. Thus, two-domain droplets emerge when this overlap region is significantly wide.

of η eventually occurs inside regions where, locally, $\phi < \phi_c$. As a result, the newly born L_1 phase is localized, making it look like it nucleates from the L_3 phase. After this, phase separation of ϕ occurs over the whole system; again, the separation of η occurs following that of ϕ, and the L_1 phase percolates.

Then we discuss whether the residence of the colloidal particles is induced by the *S-A* transition or by another phenomenon in the $C_{10}E_3$ solution with colloidal particles. Our simulation results suggest that the sponge phase is symmetric; that is, the *S-A* transition does not occur in this system. Thus, the colloidal particles are considered to reside before transformation of the membranes. Note that membrane structures are preferentially formed near substrates such as particles due to wetting [26]. After this, the lamella phase is formed over the whole system, combining with the structure around the particles. It might be expected that the sequential dynamics described above can thus affect the spatial distribution of colloidal particles. To understand the mixing effect of the colloidal particles completely, we thus consider that the spatial distribution of colloidal particles in the lamella phase should be investigated from the view of the dynamical process.

Finally, we note an analogy between the membrane system and a chiral system. In order to form connected droplets with different parities, the correlation length of the concentration needs to be longer than that of the parity. To realize this condition, it is expected that systems need to be close to a critical point. For example, the critical point for a liquid-liquid phase separation is located below the melting temperature in protein systems [27] and in molecular systems [28]. In such systems, it might be possible that topological boundaries are induced spontaneously during self-organization. Thus, an understanding of the transition in a membrane system might lead to progress in our general understanding of systems with parity.

V. CONCLUSION

To summarize, we investigated the dynamics of the deswelling transition from a sponge phase to a dense sponge/dilute sponge coexistence phase in $C_{10}E_3$ solutions. It is known that the L_1 phase is divided into inside and outside regions, which are geometrically different but energetically equivalent. Near the binodal line, it was observed that connected droplets with both inside and outside domains are sequentially formed near the binodal line. The coarsening follows a $t^{1/3}$ law, whose exponent is the same as that for coarsening in conserved phase separation. When the system is taken far from the binodal line, growth of the fluctuations is observed, similar to that seen in spinodal decomposition. This is followed by nucleation of a droplet of the L_1 phase, even though the micelle phase is the majority phase. We also performed numerical simulations using phenomenological equations for the membrane concentration ϕ and a geometric parameter η describing the inside and the outside. Simulation results reproduced the typical behavior observed in the experiments when the correlation length of ϕ is much larger than that of η and the initial sponge phase is symmetric, $\bar{\eta} = 0$. Here, we also found that the symmetry of the sponge phase, or the existence of the symmetric breaking *S-A* transition, can easily be judged by observation of the transition from the sponge phase to the coexistence phase. This also suggests that the correlation length of the density or concentration needs to be long in order to form multidomain droplets with different parities, such as in chiral systems. From these results, our study presents progress not only in the study of membrane systems but also as a general mechanism for understanding the generation of topological boundaries between domains of different chiralities.

ACKNOWLEDGMENTS

R.K. was supported by JSPS KAKENHI (Grant No. 20H01874), and M.T. was supported by JSPS KAKENHI (Grant No. 20K14431).

R.K. conceived the project, and T.K. and Y.T. performed the experiment. T.K. and R.K. performed the numerical simulations. M.T. and R.K. considered the mechanism of the transition. R.K. wrote the manuscript.

The authors declare that they have no competing financial interests.

[1] P. G. Saffman and M. Delbrück, Brownian motion in biological membranes, Proc. Natl. Acad. Sci. USA **72**, 3111 (1975).

[2] P. F. Fahey, D. E. Koppel, L. S. Barak, D. E. Wolf, E. L. Elson, and W. W. Webb, Lateral diffusion in planar lipid bilayers, Science **195**, 305 (1977).

[3] Y. Gambin, R. Lopez-Esparza, M. Reffay, E. Sierecki, N. S. Gov, M. Genest, R. S. Hodges, and W. Urbach, Lateral mobility of proteins in liquid membranes revisited, Proc. Natl. Acad. Sci. USA **103**, 2098 (2006).

[4] M. Kleman and O. D. Lavrentovich, *Soft Matter Physics: An Introduction* (Springer, New York, 2003).

[5] G. Schmitz and G. Müller, Structure and function of lamellar bodies, lipid-protein complexes involved in storage and secretion of cellular lipids., J. Lipid Res. **32**, 1539 (1991).

[6] W. Helfrich, Steric interactions of fluid membranes in multilamellar systems, Z. Naturforsch. **33a**, 305 (1978).

[7] S. A. Safran, *Statistical Thermodynamics of Surfaces, Interfaces, and Membranes* (Addison-Wesley, New York, 1994).

[8] D. Roux, C. Coulon, and M. E. Cates, Sponge phases in surfactant solutions, J. Phys. Chem. **96**, 4174 (1992).

[9] R. Granek and M. E. Cates, Sponge phase of surfactant solutions: An unusual dynamic structure factor, Phys. Rev. A **46**, 3319 (1992).

[10] H. Tanaka, M. Isobe, and J. Yamamoto, Spontaneous Partitioning of Particles into Cellar Structures in a Membrane system, Phys. Rev. Lett. **89**, 168303 (2002).

[11] T. D. Le, U. Olsson, K. Mortensen, J. Zipfel, and W. Richtering, Nonionic amphiphilic bilayer structures under shear, Langmuir **17**, 999 (2001).

[12] Y. Iwashita and H. Tanaka, Self-organization in phase separation of a lyotropic liquid crystal into cellular, network and droplet morphologies, Nat. Mater. **5**, 147 (2006).

[13] R. Kurita, S. Mitsui, and H. Tanaka, Response of Soft Continuous Structures and Topological Defects to a Temperature Gradient, Phys. Rev. Lett. **119**, 108003 (2017).

[14] Y. Izaki, R. Kurita, and H. Tanaka, Hidden linear defects in surfactant onions revealed by coalescence into lamellar layers, Phys. Rev. Research **3**, 043094 (2021).

[15] A. Onuki, *Phase Transition Dynamics* (Cambridge University Press, Cambridge, 2002).

[16] J. Fukuda and S. Zumer, Quasi-two-dimensional skyrmion lattices in a chiral nematic liquid crystal, Nat. Commun. **2**, 246 (2011).

[17] G. Chang, B. J. Wieder, F. Schindler, D. S. Sanchez, I. Belopolski, S.-M. Huang, B. Singh, D. Wu, T.-R. Chang, T. Neupert, S.-Y. Xu, H. Lin, and M. Z. Hasan, Topological quantum properties of chiral crystals, Nat. Mater. **17**, 975 (2018).

[18] N. Nagaosa and Y. Tokura, Topological properties and dynamics of magnetic skyrmions, Nat. Nanotechnol. **8**, 899 (2013).

[19] See Supplemental Material at http://link.aps.org/supplemental/10.1103/PhysRevResearch.4.023254 for supplemental movies (Movie S1 corresponds to Fig. 2, and Movie S2 corresponds to Fig. 4).

[20] L. D. Landau and E. M. Lifshitz, *Fluid Mechanics* (Pergamon, London, 1987).

[21] M. E. Cates and D. Roux, Random bilayer phases of dilute surfactant solutions, J. Phys.: Condens. Matter **2**, SA339 (1990).

[22] C. Coulon, D. Roux, and A. M. Bellocq, Second-Order Symmetric-Asymmetric Phase Transition of Randomly Connected Membranes, Phys. Rev. Lett. **66**, 1709 (1991).

[23] P. R. ten Wolde and D. Frenkel, Enhancement of protein crystal nucleation by critical density fluctuations, Science **277**, 1975 (1997).

[24] Y. C. Shen and D. W. Oxtoby, Density functional theory of crystal growth: Lennard-Jones fluids, J. Chem. Phys. **104**, 4233 (1996).

[25] R. Kurita and H. Tanaka, Drastic enhancement of crystal nucleation in a molecular liquid by its liquid–liquid transition, Proc. Natl. Acad. Sci. USA **50**, 24949 (2019).

[26] Y. Iwashita and H. Tanaka, Surface-Assisted Monodomain Formation of an Ordered Phase of Soft Matter Via the First-Order Phase Transition, Phys. Rev. Lett. **95**, 047801 (2005).

[27] O. Galkin and G. Vekilov, Control of protein crystal nucleation around the metastable liquid-liquid phase boundary, Proc. Natl. Acad. Sci. USA **97**, 6277 (2000).

[28] R. Kurita and H. Tanaka, Critical-like phenomena associated with liquid-liquid transition in a molecular liquid, Science **306**, 845 (2004).